# Site-Directed Mutagenesis of a Catalytic Antibody: An Arginine and a Histidine Residue Play Key Roles†

Jon D. Stewart,‡ Victoria A. Roberts,§ Neil R. Thomas,‡ Elizabeth D. Getzoff,§ and Stephen J. Benkovic*,‡

*Department of Chemistry, 152 Davey Laboratory, The Pennsylvania State University, University Park, Pennsylvania 16802, and Department of Molecular Biology, The Scripps Research Institute, 10666 North Torrey Pines Road, La Jolla, California 92037*

*Received September 2, 1993; Revised Manuscript Received October 29, 1993*®

ABSTRACT: Individual residues important for ligand binding and catalytic activity were identified by computer modeling and investigated by site-directed mutagenesis for catalytic antibody 43C9, which accelerates amide hydrolysis by a factor of $10^6$. On the basis of a computer model, Tyr L32, His L91, Arg L96, His H35, and Tyr H95 were chosen for replacement by site-directed mutagenesis. To facilitate these studies, an expression system was developed in which properly folded 43C9 single-chain antibody was secreted from an engineered *Escherichia coli* host. Substitution of His L91 by Gln produced a mutant with no catalytic activity, but whose affinities for ligands were nearly the same as those of the wild-type, identifying His L91 as the nucleophile that forms the acyl intermediate implicated by previous kinetic studies. Arg L96 is also critical for catalytic activity and appears to function as an oxyanion hole for the tetrahedral transition states. Two substitutions for His H35 resulted in mutant proteins with no catalytic activity as well as altered affinities for ligands, indicating an important structural role for this residue. Substitutions for Tyr L32 and Tyr H95 were made in an attempt to improve the catalytic efficiency of 43C9. The results of these mutations allow us to propose a mechanism for 43C9-catalyzed hydrolysis: Substrate binding to 43C9 orients the scissile carbonyl group adjacent to both the His L91 and Arg L96 side chains. The imidazole of His L91 acts as a nucleophile, forming an acyl–antibody intermediate that breaks down by hydroxide attack to afford the products and regenerate the catalyst.

While there are now more than 40 examples of reactions catalyzed by antibodies, there have been far fewer detailed investigations of their mechanisms (Stewart et al., 1993; Benkovic, 1992; Lerner et al., 1991). Such studies are valuable, both for understanding the similarities and differences between antibody and enzymic catalysis and for discovering methods by which the often modest catalytic power of antibodies can be improved (Stewart & Benkovic, 1993). We have chosen antibody 43C9, which catalyzes the hydrolysis of anilide **1a** and related esters **1b–f** (Scheme 1), as a model system for the mechanistic analysis of catalytic antibodies. While the substrates for 43C9 are synthetic amides and esters, we believe that the general principles learned from this antibody can be applied to engineer antibodies that can cleave proteins site-specifically. Such targeted protein cleavage would provide a very powerful means to control biological systems *in vivo*.

Previous kinetic investigations revealed that ester and amide hydrolysis catalyzed by 43C9 follows a multistep kinetic pathway whose overall organization is similar to that of a serine protease (Benkovic et al., 1990). While the phosphonamidate hapten **4** used to induce 43C9 was designed to favor general-acid–base catalysis of tetrahedral intermediate formation and decomposition, the pH–rate profiles in both $H_2O$ and $D_2O$ indicated the presence of a steady-state intermediate in the mechanistic pathway, which decomposed in a step involving hydroxide ion (Benkovic et al., 1990). The two most likely candidates for the required species appeared to be a stabilized tetrahedral structure and a covalent acyl–antibody. However, a stabilized, symmetrical tetrahedral intermediate was rendered unlikely by the lack of $^{18}O$ exchange into unreacted **1a** and by the absence of the expected solvent isotope effect accompanying its formation (Janda et al., 1991). These results were, however, consistent with an acyl–antibody intermediate, and further support for this hypothesis came from analysis of the rates of hydrolysis for a series of para-substituted phenyl esters by means of a Hammett plot (Gibbs et al., 1992). For the uncatalyzed reaction, a $\rho$ value of +0.8 was obtained, consistent with rate-limiting attack by an anionic oxygen nucleophile, *i.e.*, hydroxide. On the other hand, the rate constant assigned to the putative acylation step for the antibody-catalyzed reaction correlated with a $\rho$ value of +2.3. This large value ruled out rate-limiting nucleophilic attack by either an anionic oxygen or sulfhydryl, as well as general-base catalysis by oxygen or nitrogen bases, but was consistent with a neutral nitrogen nucleophile (Gibbs et al., 1992). Furthermore, of the many classical side-chain-modifying reagents tested, only diethyl pyrocarbonate destroyed the catalytic activity of 43C9 (Benkovic et al., 1990). Taken together, the results of these studies support the hypothesis that both ester and amide hydrolyses catalyzed by 43C9 proceed through an acyl–antibody intermediate formed with a histidine side chain. Cloning and sequencing of the genes encoding the Fab fragment of 43C9 revealed that the protein contained two histidines, one each in the light and heavy chains (Gibbs et al., 1991).

We wished to correlate the results of the previous kinetic studies of 43C9 with its structure in order to understand the catalytic mechanism at the molecular level. Thus, our site-directed mutagenesis studies of 43C9 had three major goals. First, we hoped to identify those residues that were critical for catalysis as well as those that did not play a direct role. Second, we hoped to improve the catalytic activity of 43C9 by introducing side chains that might act as general acids.

† This work was supported by a Helen Hay Whitney Foundation postdoctoral fellowship to J.D.S., by a NATO postdoctoral fellowship to N.R.T., and by grants from the Office of Naval Research (N00014-91-J-1593 and N00014-91-J-1885).

‡ The Pennsylvania State University.

§ The Scripps Research Institute.

® Abstract published in *Advance ACS Abstracts,* February 1, 1994.

0006-2960/94/0433-1994$04.50/0 

Scheme 1

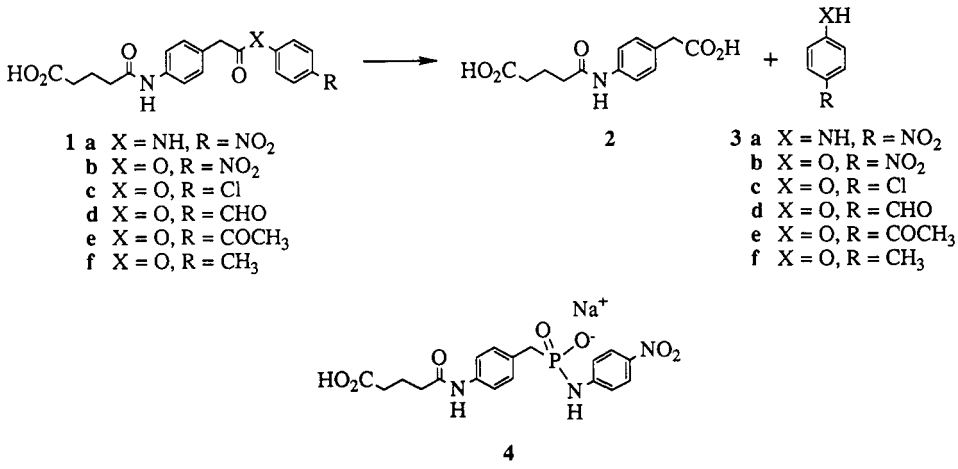


1 a X = NH, R = $NO_2$
b X = O, R = $NO_2$
c X = O, R = Cl
d X = O, R = CHO
e X = O, R = $COCH_3$
f X = O, R = $CH_3$

2

3 a X = NH, R = $NO_2$
b X = O, R = $NO_2$
c X = O, R = Cl
d X = O, R = CHO
e X = O, R = $COCH_3$
f X = O, R = $CH_3$

4

Finally, since no high-resolution X-ray or NMR structure is available for 43C9, a computer model of the 43C9 Fv[1] fragment with bound hapten **4** had been previously constructed on the basis of antibodies whose crystal structures have been determined (Roberts et al., 1994). Thus, we expected that the results of our mutagenesis studies would provide further support for the 43C9 Fv model or suggest areas that required further refinement.

## MATERIALS AND METHODS

*General.* All kinetic and ligand binding measurements were performed at 25 °C in a buffer containing 100 mM ACES, 50 mM Tris, and 50 mM CAPS (ATC buffer) at the indicated pH value. Routine DNA and bacterial manipulations were performed by standard techniques (Sambrook et al., 1989), and *Escherichia coli* DH5$\alpha$ or JM105 was used for the propagation of plasmid DNA. *E. coli* BL21 (genotype *hsdS*, *gal*) and plasmids p4.1 and pTG119 were generous gifts from Robert La Polla (R. W. Johnson Pharmaceutical Research Institute). Restriction and DNA-modifying enzymes were purchased from New England Biolabs, Bethesda Research Labs, or Boehringer-Mannheim. DNA sequences were determined using the Sequenase kit (U.S. Biochemical) according to the manufacturer's instructions. Oligonucleotides for mutagenesis and DNA sequencing were obtained from American Synthesis, Inc. or the Midland Certified Reagents Co. and were used without prior purification. The sequences of primers used for mutagenesis are shown in Table 1. All materials for the polymerase chain reaction were obtained from Perkin-Elmer Cetus. Phosphonamidate hapten **4**, *p*-chlorophenyl ester **1c**, and acid **2** were synthesized as described previously (Gibbs et al., 1992; Janda et al., 1988).

*Single-Chain Antibody Isolation.* A single colony of freshly transformed *E. coli* BL21 (pTG119, pJS118) was used to inoculate 25 mL of LB + 10 $\mu$g/mL tetracycline and 30 $\mu$g/mL kanamycin. After the culture grew overnight at 37 °C, portions were diluted 1:100 into two 1-L volumes of LB + 10 g/L MOPS, 10 $\mu$g/mL tetracycline, and 30 $\mu$g/mL kanamycin. Before autoclaving, the pH of the medium was adjusted to pH 7.5 with NaOH. The cultures were grown at 37 °C until they reached $OD^{600}$ = 1.0, and then they were cooled to room temperature for 15 min. IPTG was added to a final concentration of 2 mM, and the cultures were shaken for 16–18 h at room temperature. The cells were then removed by centrifugation (7000*g* for 30 min at 4 °C), and PMSF was added to a final concentration of 0.5 mM. The following steps were performed at 4 °C. The growth medium (which contained the single-chain antibody) was concentrated to approximately 80 mL using a Mini-Tan apparatus (Millipore Corp.) equipped with either two or four 10 000 NMWL membranes. The resulting solution was concentrated further to approximately 10 mL with an Amicon YM-10 membrane, and then it was dialyzed against 3 × 1 L of 20 mM Na MOPS/0.4 mM $Ca(OAc)_2$ (pH 6.3). The dialyzed material was concentrated to ≤10 mL with an Amicon YM-10 membrane, centrifuged at 20000*g* for 15 min at 4 °C to remove precipitated material, and then chromatographed on a 21 × 250 mm PolyCAT A column (Nest Group) that had been equilibrated with 40 mM Na MOPS/1 mM $Ca(OAc)_2$ (pH 6.3). A Pharmacia FPLC system was used for this chromatography. After loading, the column was eluted with a linear gradient formed by 750 mL of the starting buffer and 40 mM Na MOPS/25 mM $Ca(OAc)_2$ (pH 7.5). A flow rate of 4 mL/min was used throughout. Fractions containing the single-chain antibody were pooled and concentrated using an Amicon YM-10 membrane and then dialyzed against ATC buffer (pH 8.0) and stored at 4 °C. Residual material was removed from the column by washing with 3 column vol of 40 mM Na MOPS/100 mM $CaCl_2$ (pH 7.5).

*Fluorescence Titrations.* The thermodynamic binding affinities of ligands ($K_D$ values) were determined at pH 7.5 by following the quenching of the intrinsic antibody fluorescence at 340 nm upon excitation at either 280 or 290 nm on an Aminco SLM 8000 spectrofluorimeter as a function of added ligand. The observed quenching was corrected for inner filter effects by the simultaneous titration of a tryptophan standard solution. Whenever possible, the antibody concentration was less than the $K_D$ of the ligand (except in the case of active-site titrations). The data were fit to a quadratic equation using a nonlinear least-squares computer program as previously described (Taira & Benkovic, 1988). The data were also plotted in Scatchard form to verify the expected 1:1 ligand:antibody stoichiometry.

*Steady-State Kinetics.* Single-chain antibody concentrations were determined by active-site fluorescence titrations

[1] Abbreviations: Fv, IgG fragment consisting of the variable regions of both the light and heavy chains; single-chain Fv, Fv fragment in which the two chains are covalently joined by a 14 amino acid linker peptide; ACES, *N*-(2-acetamido)-2-aminoethanesulfonic acid; CAPS, 3-(cyclohexylamino)-1-propanesulfonic acid; $OD^{600}$, optical density at 600 nm; IPTG, isopropyl $\beta$-D-thiogalactopyranoside; PMSF, phenylmethanesulfonyl fluoride; NMWL, nominal molecular weight limit; MOPS, 4-morpholinepropanesulfonic acid; FPLC, fast protein liquid chromatography; SCA, single-chain antibody; CDR, complementarity determining region; PCR, polymerase chain reaction.

with the phosphonamidate hapten using a single-chain antibody concentration at least 10-fold higher than the $K_D$ value. Initial velocities were measured for *p*-chlorophenyl ester **1c** hydrolysis at pH 8.5 using either a Cary 118 or a Cary 1 UV–visible spectrophotometer, as described previously (Gibbs et al., 1991). When determining whether a given protein possessed catalytic activity, the concentration of substrate **1c** was fixed at 2 mM (near the solubility limit for **1c**) and the amount of single-chain antibody was varied. Steady-state kinetic parameters were determined for the wild-type, Y-L32-H, and Y-H95-F proteins as described by Gibbs et al. (1991). These reactions contained 0.20, 0.75, and 1.0 μM single-chain antibody for measurements on the wild-type, Y-L32-H, and Y-H95-F mutant proteins, respectively.

*Rapid Kinetic Studies.* Kinetic studies of the Y-H95-H single-chain antibody were performed on an Applied Photophysics stopped-flow spectrophotometer. In these experiments, a varying amount of Y-H95-H single-chain antibody (in 2× ATC buffer) was rapidly mixed with a fixed concentration of *p*-nitrophenyl ester **1b** (dissolved in a weak acidic buffer to prevent decomposition), and the absorbance change at 350 nm was monitored. The isosbestic point for *p*-nitrophenol was chosen to avoid artifacts caused by tight binding of this product by the antibody (Benkovic et al., 1990). One syringe contained 150 μL of 4× ATC (pH 7.3), 50 μL of distilled water, Y-H95-H single-chain antibody in 1× ATC (pH 8.0) (up to 200 μL), and sufficient 1× ATC (pH 8.0) to give a final volume of 400 μL. This mixture had a final pH value of 7.45. The other syringe contained 380 μL of 5 mM ACES (pH 4.0), 16 μL of dioxane, and 4.0 μL of a 20 mM stock solution of the substrate in dioxane. This substrate concentration was slightly below the solubility limit for **1b** at pH 4.0. After mixing, the reaction was followed for 50 s. A molar extinction coefficient for *p*-nitrophenol of 3500 $M^{-1}$ was calculated for the path length of this instrument. The absorbance data were fit to the multistep mechanism described for the wild-type protein using the computer program KINSIM (Barshop et al., 1983).

*Sequence Numbering.* We used the consensus nomenclature of Kabat et al. (1991) for numbering the residues of the single-chain antibody. The three CDR loops of the light chain are designated L1, L2, and L3, and those of the heavy chain are designated H1, H2, and H3.

*Construction of a Computer Model of 43C9 with Bound Amide Substrate.* The model of the 43C9 variable region with bound substrate was built from the previously constructed model of 43C9 with bound hapten **4** (Roberts et al., 1994). The *p*-nitrophenyl phosphonamidate group of the hapten was replaced by the *p*-nitroanilide group from alanylalanine-*p*-nitroanilide hydrochloride (from the Cambridge database of small molecules), providing a model of substrate **1a** with geometry similar to that of the hapten. The substrate was docked into the 43C9 antibody binding pocket in a manner similar to the antigen, and the fit was refined by energy minimization with the Discover program (Biosym Technologies, Inc.). The residues surrounding the substrate (Tyr L32, Phe L50, His L91, Arg L96, Asn H33, Val H34, His H35, Met H50, Ile H51, Trp H52, Val H93, Ser H94, and residues H95–H102, which make up CDR3 of the heavy chain) were constrained to their initial coordinates with a harmonic forcing constant of 100 kcal $Å^{-1}$, and the rest of the antibody was held fixed. Substrate and surrounding residues were minimized to a final maximum derivative of less than 10.0 kcal $mol^{-1}$ $Å^{-1}$, using the steepest descent minimizer, and then to a final maximum derivative of less than 1.0 kcal $mol^{-1}$ $Å^{-1}$, using the Broydon-Fletcher-Goldfarb-Shanno minimizer to produce the final model.

The geometry of the 43C9 His H35 side chain was compared with those of known antibodies by using our antibody structural database, which contains the crystallographically determined $V_H$ structures superimposed onto the $V_H$ of the McPC603 antibody. Specifically, the $V_H$ of 43C9 was superimposed onto those of known structures by its conserved backbone structure, the main-chain atoms of residues H3–H12, H17–H25, H33–H52, H56–H60, H68–H82, H88–H95, and H102–H112, using the program RMSN (Roberts et al., 1994).

## RESULTS

The efficient expression of 43C9 in a bacterial host represented an important goal of this work because it would allow the consequences of specific mutations to be assessed rapidly. We chose the single-chain Fv form of 43C9 (Gibbs et al., 1991) for the present study for two main reasons. First, it has not been possible to express functional IgG molecules in bacterial hosts, whereas single-chain Fv's have been successfully produced in such hosts by a number of groups, albeit with varying degrees of efficiency [for a review, see Whitlow and Filpula (1991)]. Second, the small size of the single-chain Fv (approximately 27 kDa) and the possibility for isotopic labeling should allow future studies of this antibody by NMR or X-ray crystallography techniques [for example, see McManus and Riechmann (1991) and Riechmann et al. (1991)]. It has previously been demonstrated that the kinetic parameters of the 43C9 single-chain Fv were essentially identical to those of the intact monoclonal antibody (Gibbs et al., 1991).

Site-directed mutagenesis studies of the 43C9 single-chain antibody required an improved expression system. In the original Genex method, the protein was produced as an insoluble inclusion body from which the single-chain antibody was extracted under denaturing conditions and then refolded prior to chromatographic purification (Gibbs et al., 1991). While the Genex method was effective for several other single-chain antibodies (Whitlow & Filpula, 1991), it performed poorly in the case of 43C9 (100 μg of purified protein per liter of culture). In addition, the large volumes required for refolding made the method inconvenient on a laboratory scale. We therefore sought an alternative expression system in which the single-chain antibody would be directly expressed in properly folded form.

We developed a new, soluble expression system for the 43C9 single-chain antibody by fusing its structural gene (*SCA*) to a bacterial leader sequence (*pelB*) under control of a bacteriophage T3 promoter. The expression plasmid, pJS118, was constructed in several steps (Scheme 2). We chose plasmid p4.1, which confers tetracycline resistance, for our expression vector because it has been successfully used to express the Fab fragment of 43C9 in soluble form (Posner et al., 1993). The plasmid contains the bacteriophage T3 promoter and the *pelB* leader sequence, along with restriction sites useful for subcloning an antibody light-chain Fab gene. Restriction sites appropriate for the p4.1 vector were introduced at the beginning (*Sac*I) and end (*Xba*I) of the *SCA* gene in a single subcloning process that yielded pJS117. The *Sac*I site was introduced by replacing the 5′-end of the *SCA* gene (from pGX5526, the original Genex expression plasmid) with the corresponding section of the 43C9 Fab light-chain gene (from pNPN) using the unique, internal *Kpn*I site within the light-chain portion of the *SCA* gene. This was possible since these DNA fragments differed only in the restriction site present

Scheme 2

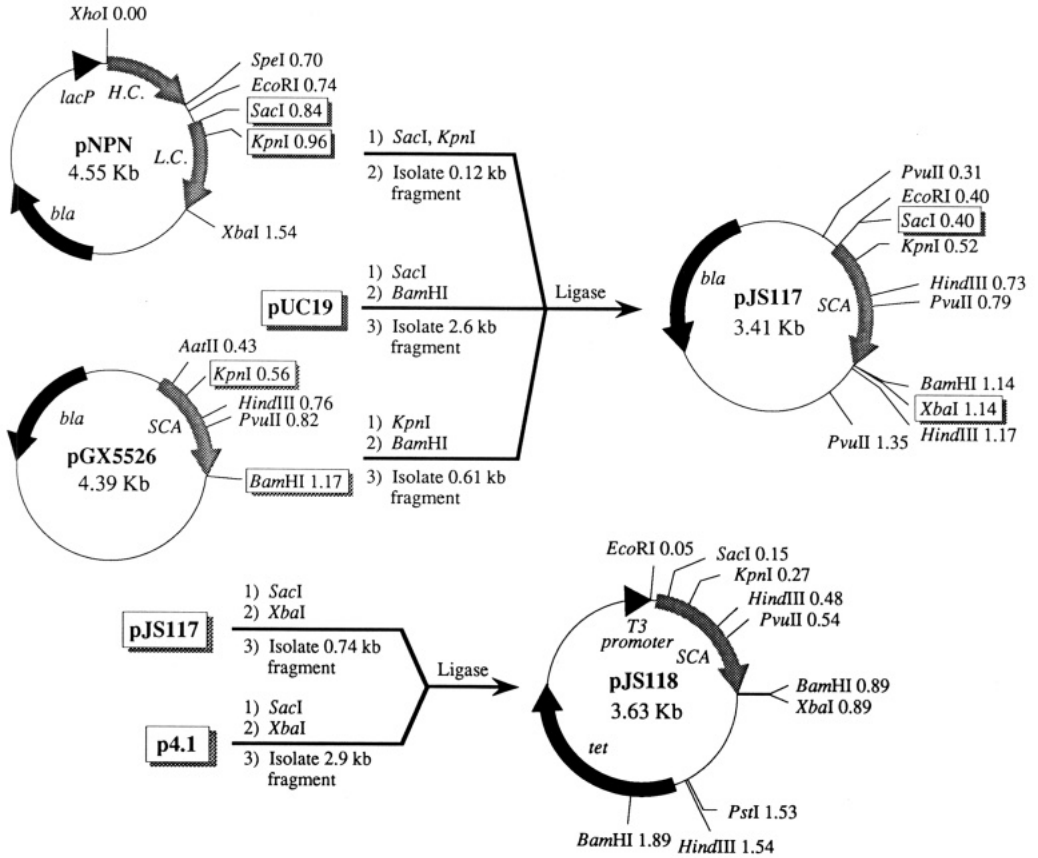


at the 5′-end of the respective genes. The required *Xba*I site was introduced by reassembling the *SCA* gene in a three-component ligation reaction with *Sac*I,*Bam*HI-cleaved pUC19 (Yanisch-Perron et al., 1985). In this vector, an *Xba*I site was present in the polylinker region downstream from the *Bam*HI site used for cloning the *SCA* gene. The overexpression plasmid, pJS118, was constructed by subcloning the *SCA* gene from pJS117 as a *Sac*I,*Xba*I cassette into p4.1. The structure of pJS118 was verified by restriction mapping, and the *SCA* gene was sequenced near the *Sac*I site to ensure that the *pelB* leader sequence was properly fused to the single-chain antibody gene.

The mutant single-chain antibody proteins were isolated and purified by the same procedure used for the wild-type protein described here. The overexpression strain for the wild-type single-chain antibody was created by transforming *E. coli* BL21 (pTG119) with pJS118 and selecting colonies for resistance to both tetracycline and kanamycin. Plasmid pTG119, which encoded the bacteriophage T3 RNA polymerase gene under control of the *lacUV5* promoter, conferred kanamycin resistance and was readily lost in the absence of kanamycin selection. The doubly transformed strain was grown in rich medium at 37 °C to the midlog phase ($OD^{600}$ = 1.0). The cultures were then cooled to room temperature and induced by adding IPTG to a final concentration of 2 mM. Induction was performed at room temperature to avoid cell lysis (Posner et al., 1993). After induction, very little single-chain antibody was found in the periplasmic space; most was found in the growth medium. This probably resulted from nonspecific leakage of the periplasmic contents rather than specific transport, since many other proteins were also found in the growth medium. We were unable to determine the fraction of properly folded single-chain antibody in the growth medium. Measurement of the concentration of active single-chain antibody by hapten binding with ELISA detection with a polyclonal rabbit anti-43C9 Fab antiserum was unreliable due to the cross-reactivity of the antiserum with other *E. coli* proteins. In addition, the presence of bacterial proteases and the relatively small amount of single-chain antibody present made quantitative assays of esterase activity impossible. However, on the basis of hapten binding and catalytic activity, we believe that virtually all of the *purified* single-chain antibody is properly folded.

The single-chain antibody could be readily isolated from the growth medium after a concentration step (Figure 1). Although the single-chain antibody could be concentrated from the growth medium either by ultrafiltration or by adsorption onto phenyl-Sepharose, the yield of purified single-chain antibody was approximately 20-fold lower when phenyl-Sepharose was employed. After concentration, the protein solution was dialyzed against a low-salt buffer, followed by chromatography on a PolyCAT A cation-exchange column with a linear $Ca^{2+}$ and pH gradient (Gibbs et al., 1991). Highly purified single-chain antibody was eluted from this column. The appropriate fractions were pooled, concentrated, and dialyzed into ATC buffer (pH 8.0) for storage at 4 °C. We have consistently obtained 600–700 μg of purified wild-type single-chain antibody per liter of culture, but the yields of some of the mutant proteins were up to 10-fold lower than this amount.

Residues targeted for site-directed mutagenesis were chosen on the basis of computer modeling and previous kinetic studies. The model of the 43C9 antibody Fv fragment was originally constructed with bound antigen (Roberts et al., 1994). To identify residues located near the scissile bond of the substrate, *p*-nitroanilide **1a** was docked into the coordinates of the 43C9 Fv fragment (Figure 2). Close inspection of this model suggested that only one of the two histidine residues of 43C9 seemed likely to play a role in the catalytic mechanism. Specifically, the Nδ of the light-chain histidine residue (L91)

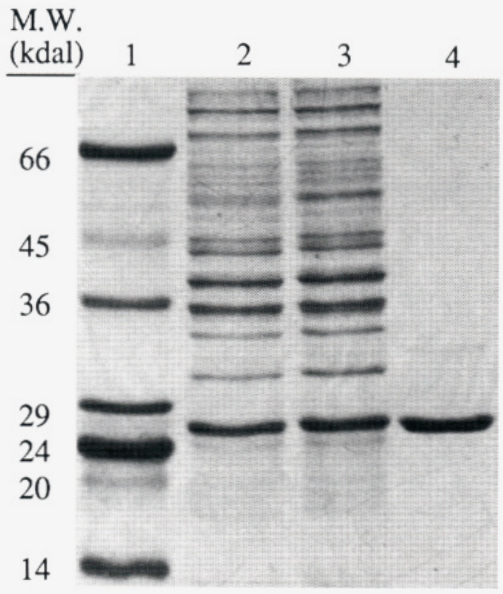


FIGURE 1: Purification of the wild-type 43C9 single-chain antibody: lane 1, molecular weight standards; lane 2, concentrated growth medium from induced BL21 (pTG119, pJS118); lane 3, after dialysis into low-salt buffer; lane 4, after chromatography on a PolyCAT A column.

was located *ca.* 4.5 Å from the carbonyl carbon, and its geometry was consistent with the stereoelectronic factors governing nucleophilic attack. To test the catalytic role of His L91, it was replaced with glutamine. While this substitution would retain some of the hydrogen-bonding patterns of histidine, it would remove any propensity for nucleophilic attack on the substrate. The heavy-chain histidine (H35), on the other hand, was located at the bottom of the antigen binding pocket and appeared to play a structural, rather than a catalytic, role. Following similar logic, His H35 was replaced with asparagine in an effort to retain some hydrogen-bonding ability at this position. However, since the H-H35-N mutant was catalytically inactive (*vide infra*), we also replaced His H35 with phenylalanine since the side chains of these residues occupy approximately the same volumes. While previous kinetic studies on 43C9 showed no evidence for participation by the side chain of a tyrosine residue, the close proximity of both Tyr L32 and Tyr H95 to the bound substrate suggested that substitutions at these positions might be used to improve the catalytic efficiency of 43C9. In addition to implicating a histidine side chain in catalysis, the large $\rho$ value of +2.3 found in the linear free energy plot indicated that the leaving group departed with nearly a full negative charge and that 43C9 did not employ general-acid catalysis in its mechanism. By replacing Tyr L32 and Tyr H95 with histidine, a proton source would be located near the leaving group and the tetrahedral intermediate, respectively. In addition, Tyr H95 was replaced with phenylalanine to determine whether its hydroxyl was critical, either for catalysis or for antibody structure.

Site-directed mutagenesis was performed on the single-chain antibody (*SCA*) gene by the overlap extension method, as described by Pease (Ho et al., 1989). The mutation of His L91 to Gln is presented as an example (Scheme 3). Plasmid pJS108 contained the 0.20-kb *Kpn*I–*Hin*dIII fragment of the *SCA* gene (which encoded amino acids L36–L104) subcloned between these sites in pUC18. Site-directed mutagenesis was performed on this 0.20-kb fragment rather than on the full *SCA* gene to minimize the amount of subsequent DNA sequencing. Two separate PCR amplifications were performed on pJS108 using either primer H-L91-Q For plus pUC18 Rev or primer H-L91-Q Rev plus pUC18 For (Table 1). In each reaction, the first primer annealed within the *SCA* gene fragment and encoded the H-L91-Q mutation, while the second annealed within the vector region of pJS108. These linear

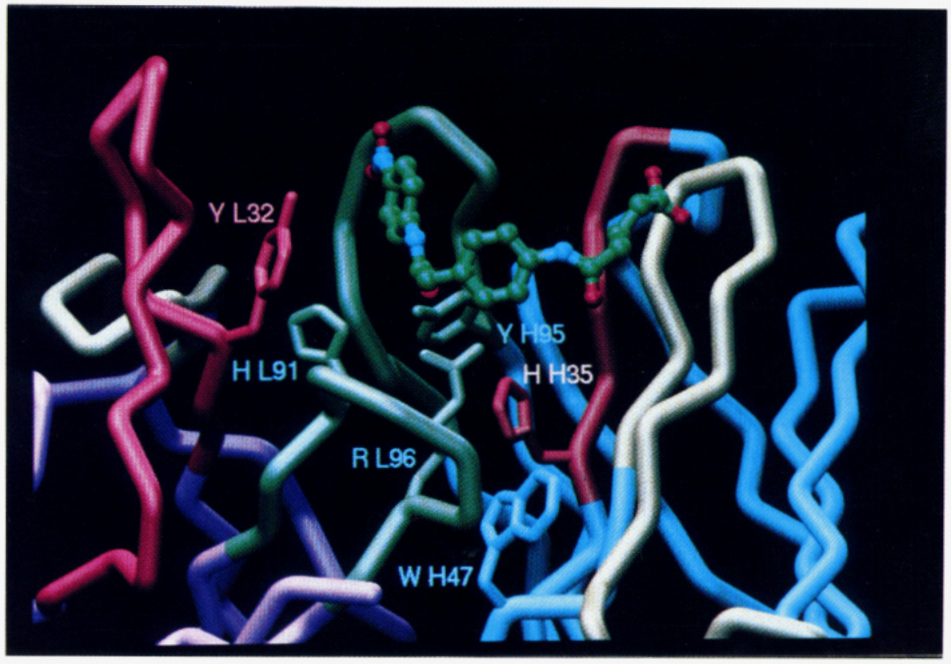


FIGURE 2: Complex of the 43C9 Fv with bound substrate showing antibody residues that lie near the substrate. The 43C9 $V_L$ (purple, C$\alpha$ backbone of framework residues) is on the left, and the 43C9 $V_H$ (blue, C$\alpha$ atoms of framework residues) is on the right. The 43C9 sequence is numbered as in Kabat et al. (1991) with L1 and H1 (red), L2 and H2 (yellow), and L3 and H3 (green). The substrate is shown as a ball-and-stick model with colored atoms: C, green; N, blue; O, red. The side chains of L1 residue Tyr L32 (red), L3 residues His L91 and Arg L96 (green), and H3 residue Tyr H95 (green) contact substrate. The lone pair on the N$\delta$ of His L91 extends toward the reactive carbonyl of the substrate. The side chain of H1 residue His H35 (red) does not contact the substrate but underlies residue Arg L96, which is critical for catalysis (Roberts et al., 1994), and residue Tyr H95. Residue Trp H47, which is buried in the $V_L/V_H$ interface, orients the His H35 side chain.

Scheme 3

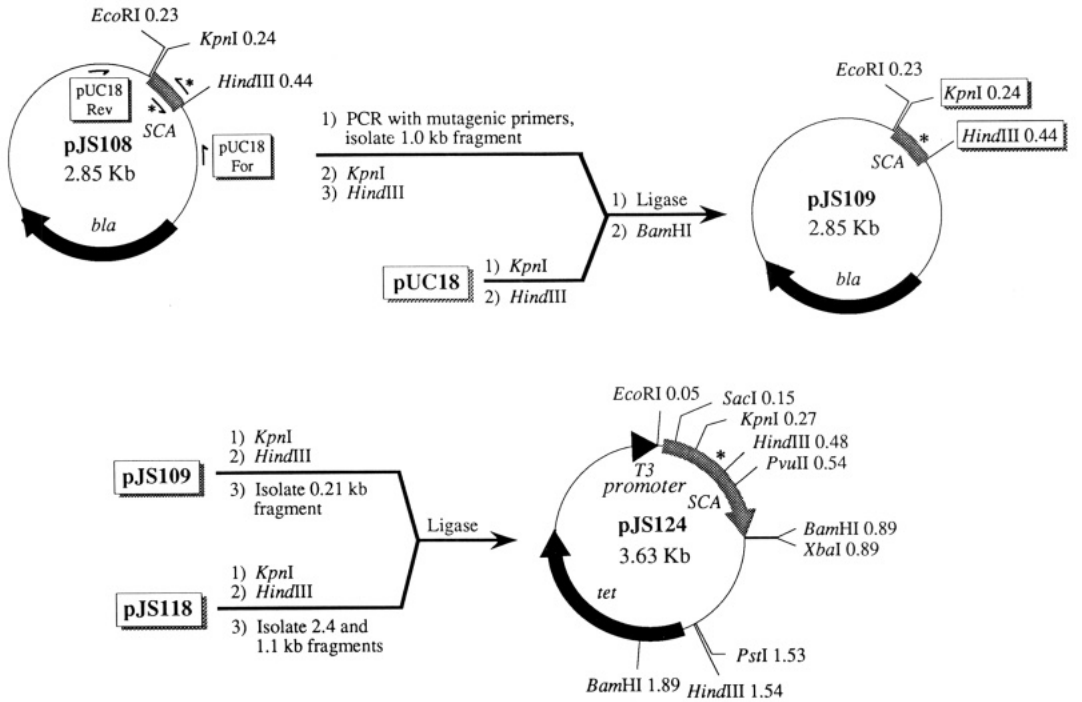


Table 1: Sequence of Primers Used for Site-Directed Mutagenesis

| name | sequence |
|---|---|
| pUC18 For | ACG CCA GCA ACG CGG |
| pUC18 Rev | ACC TCT GAC ACA TGC AG |
| Y-L32 Random | G CTG GTA CCA GGC CAA NTB GTT CTT TTG ATT |
| H-L91-Q For | TGT CAG CAA CAA TAT AGG GCT |
| H-L91-Q Rev | AGC CCT ATA TTG TTG CTG ACA |
| H-H35-F For | G GGG AAC GTT TTT TGG GTT CGC CAG TCT CCA GGA AAG |
| H-H35-F Rev | G GCC AAC GTT ATA TCT GGA TAA TGA GAT CCC AGA |
| H-H35-N For | TAT AAT GTA AAC TGG GTT CGC |
| H-H35-N Rev | GCG AAC CCA GTT TAC ATT ATA |
| Y-H95-F For | TAC TGT GTC AGT TTT GGT TAC GGC GGG |
| Y-H95-F Rev | CCC GCC GTA ACC ATG ACT GAC ACA GTA |
| Y-H95-H For | TAC TGT GTC AGT CAT GGT TAC GGC GGG |
| Y-H95-H Rev | CCC GCC GTA ACC ATG ACT GAC ACA GTA |

DNA fragments were purified by agarose gel electrophoresis, mixed, and amplified using the two vector primers pUC18 For and pUC18 Rev. In this amplification step, the DNA chains of the up- and downstream fragments of the *SCA* gene formed heterodimers by annealing in the complementary region of the introduced mutation, and these overlapping chains acted as primers for self-synthesis. PCR amplification with the two vector primers yielded the reassembled 1.0-kb DNA fragment located between the primers. This region contained the complete 0.20-kb *SCA* gene fragment with the H-L91-Q mutation present in both strands. This 1.0-kb fragment was purified by agarose gel electrophoresis and digested with *Kpn*I and *Hin*dIII. Without further purification, the 0.20-kb *SCA* gene fragment was cloned into pUC18 between these sites. DNA sequencing of the entire *SCA* gene fragment from random clones identified a plasmid, designated pJS109, that contained the desired H-L91-Q mutation and no others. The *SCA* gene fragment was isolated from pJS109 as a *Kpn*I,-*Hin*dIII cassette and was used to replace the corresponding wild-type segment of pJS118 to produce pJS124. The structure of pJS124 was verified by restriction mapping and by DNA sequencing to ensure that it encoded only the desired mutation.

Mutations at position L32 were introduced by a method that took advantage of the proximity of this codon to a unique *Kpn*I site within the light chain gene segment. A primer (Y-L32 Random) was designed that spanned both the *Kpn*I site and codon L32 (Table 1). This primer contained a mixture of bases at two positions to replace Tyr L32 by Asn, Asp, Gln, Glu, His, or Lys. This mixture of mutants was produced by PCR amplification of pJS117 with Y-L32 Random and pUC18 Rev. The resulting 0.50-kb product encoded a mixture of codons at position L32 with the *SCA* gene fragment flanked by an *Sac*I and a *Kpn*I site. After agarose gel purification, this DNA was sequentially digested with *Sac*I and *Kpn*I, and then the mixture was ligated with the large *Sac*I–*Kpn*I fragment of pJS118. After transformation, plasmids encoding the desired replacements for Tyr L32 were identified by sequencing random clones. In this way, pJS135, which encoded the Y-L32-H mutant of the 43C9 single-chain antibody, was isolated.

Overexpression plasmids encoding the H-H35-N, H-H35-F, Y-H95-H, and Y-H95-F mutants were constructed by procedures similar to those described above. For these, pNT101 was used as the template for the PCR amplifications since it contained the *Hin*dIII–*Bam*HI fragment of the *SCA* gene (which encoded amino acids L103–H112) subcloned between these sites of pUC18 (Figure 3).

Since it was expected that several of the mutant single-chain antibodies would lack catalytic activity, it was essential to verify that their inactivity was not simply a consequence of large structural perturbations within these proteins. The thermodynamic binding of ligands—hapten **4** and products acid **2** and *p*-nitrophenol **3b**—was therefore determined for each protein by following the quenching of intrinsic protein fluorescence (excitation $\lambda = 280$ or 290 nm, emission $\lambda = 340$ nm) upon ligand titration (Taira & Benkovic, 1988). The $K_D$ values obtained are listed in Table 2. The affinity of an antibody mutant for hapten **4** provides the most direct indication of nativelike structure. Furthermore, the retention

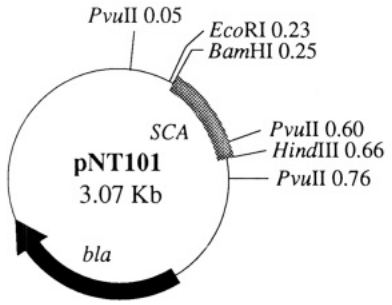


FIGURE 3: Partial restriction map of pNT101. This plasmid contains a 0.41-kb fragment of the *SCA* gene cloned between the *Bam*HI and *Hin*dIII sites of pUC18, which encodes the C-terminal 135 amino acids of the 43C9 single-chain antibody.

Table 2: Thermodynamic Dissociation Constants for Ligand Binding to Mutant and Wild-Type 43C9 Single-Chain Antibodies at pH 7.5, 25 °C

| | | $K_D$ | | |
|---|---|---|---|---|
| protein | plasmid | hapten (nM) | acid ($\mu$M) | phenol ($\mu$M) |
| wt | pJS118 | ≤1 | 15 ± 1 | 0.6 ± 0.1 |
| Y-L32-H | pJS135 | 0.67 ± 0.35 | 12 ± 3 | 0.38 ± 0.09 |
| H-L91-Q | pJS124 | ≤1 | 17 ± 3 | 0.53 ± 0.16 |
| H-H35-N | pNT116 | 16 ± 2 | 100 ± 10 | 5.5 ± 1.5 |
| H-H35-F | pJS157 | 13 ± 6 | 15 ± 2 | 1.4 ± 0.1 |
| R-L96-Q[a] | pJS129 | 16 ± 4 | 31 ± 8 | 0.96 ± 0.16 |
| Y-H95-F | pJS147 | ≤2 | 25 ± 8 | 0.65 ± 0.22 |
| Y-H95-H | pJS141 | ≤2 | 21 ± 6 | 0.70 ± 0.18 |

[a] Roberts et al. (1994).

Table 3: Steady-State Kinetic Parameters for Wild-Type and Mutant 43C9 Single-Chain Antibodies

| | protein | | | |
|---|---|---|---|---|
| | wt Mab[a] | wt | Y-L32-H | Y-H95-F |
| $K_M$ ($\mu$M) | 630 ± 139 | 470 ± 160 | 1300 ± 100 | 990 ± 90 |
| $k_{cat}$ ($s^{-1}$) | 0.40 ± 0.03 | 0.46 ± 0.05 | 0.17 ± 0.01 | 0.18 ± 0.01 |

[a] Gibbs et al. (1991).

of hapten binding ability implies the retention of substrate binding ability. The binding of products was also measured for each antibody mutant in an attempt to localize structural perturbations within the binding site. According to the model structure (Roberts et al., 1994), the hapten binds in an "L"-shaped conformation, with the two aromatic rings separated by an approximately 90° bend that occurs at the benzylic carbon. Acid **2** and *p*-nitrophenol **3b** correspond to each of the two legs of the hapten. Of course, the assumption that these ligands bind to the mutant proteins in the same manner as they do to the wild-type is implicit in this analysis. Interestingly, the $K_D$ values for the mutant proteins were nearly the same as those for the wild-type, with the exception of the H-H35-N and H-H35-F mutants.

The catalytic activities of the above proteins were assessed by measuring the initial rates of hydrolysis of 2 mM *p*-chlorophenyl ester **1c** in the presence and absence of each single-chain antibody. This substrate concentration, which was approximately 4-fold higher than the $K_M$ value for the wild-type protein, approached the solubility limits for **1c**. The wild-type, Y-L32-H, and Y-H95-F mutant proteins all possessed appreciable catalytic activity, and their steady-state kinetic parameters are listed in Table 3. The Y-H95-H protein possessed low, but reproducible, *p*-chlorophenyl esterase activity. On the other hand, the H-L91-Q, R-L96-Q, H-H35-N, and H-H35-F mutants had no detectable catalytic activities when assayed at protein concentrations up to at least 2.5 $\mu$M.

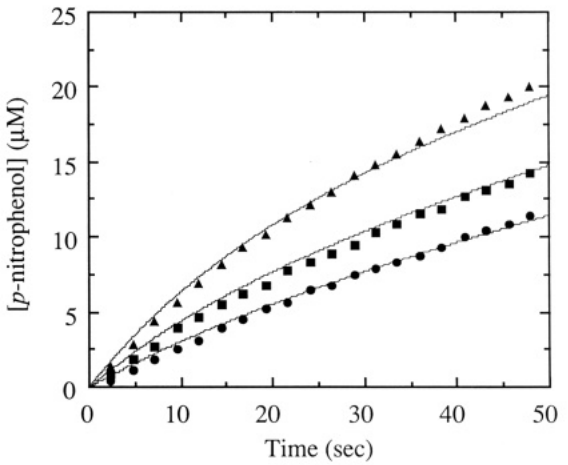


FIGURE 4: Hydrolysis of *p*-nitrophenyl ester **1b** catalyzed by the Y-H95-H 43C9 single-chain antibody: solid lines, concentrations calculated by KINSIM; symbols, measured concentration data (●, [Y-H95-H SCA] = 3.75 $\mu$M; ■, [Y-H95-H SCA] = 7.0 $\mu$M; ▲, [Y-H95-H SCA] = 12 $\mu$M).

Given the background rate and the sensitivity of our assay, we estimate that $k_{cat}$ is reduced by factors of >50-fold in these cases.

The catalytic activity of the Y-H95-H mutant was examined in more detail by stopped-flow methods to determine whether the acyl intermediate could be detected during the first turnover. The *p*-nitrophenyl ester was chosen for these studies rather than the *p*-chlorophenyl ester because it was expected to bind much more tightly to the antibody [$K_M$ values for **1b** and **1c** are 53 and 720 $\mu$M, respectively, for the wild-type (Gibbs et al., 1992)]. In addition, the high reactivity of **1b** should make the acylation rate extremely rapid [≥180 $s^{-1}$ for the wild-type (Gibbs et al., 1992)], and the extinction coefficient of *p*-nitrophenol is approximately 3-fold higher than that of *p*-chlorophenol at their isosbestic points. While the curvature of the data (Figure 4) initially suggested that the acyl intermediate accumulated to significant levels as the result of a lowered deacylation rate, a close examination of the data showed that this was not the case. Most importantly, the observed steady-state rates varied with antibody concentration, inconsistent with single-turnover kinetics. The experimental data were therefore fit by a simulation of the multistep mechanism originally proposed for the wild-type protein (Scheme 4), and the wild-type rate constants (Gibbs et al., 1992) were used with the following exceptions. The off-rates for acid and *p*-nitrophenol ($k_4$ and $k_5$, respectively) were adjusted slightly in order to match the observed $K_D$ values for these ligands, and the rate of the background reaction was set to the value observed under our conditions ($1.45 \times 10^{-3}$ $s^{-1}$). The rate constants $k_2$, $k_{-2}$, and $k_3$ were varied in order to fit the experimental data for these substrate concentrations and provided a unique value for the forward rate term, $(k_2/k_{-2})k_3$, of 0.068 $s^{-1}$, which is 4-fold less than the value of the wild-type. Nevertheless, deacylation remains rapid relative to acylation in this mutant since no burst of *p*-nitrophenol was observed at short reaction times (≤120 ms). As in the case of wild-type antibody, the decrease in catalytic rate over time results from the accumulation of the inhibitory *p*-nitrophenol product.

## DISCUSSION

The ability to directly express a catalytic antibody fragment in soluble form using a bacterial host has greatly expanded our ability to dissect its mechanism by site-directed mu-

Scheme 4

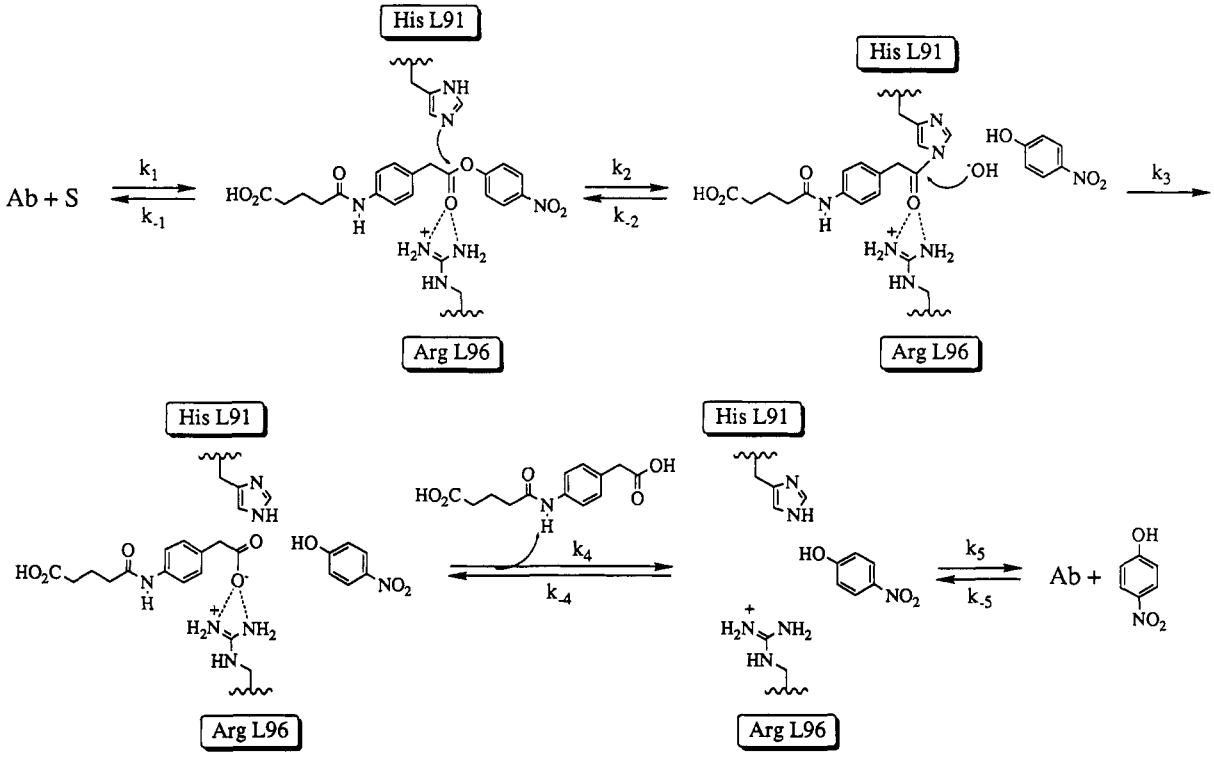


tagenesis (Glockshuber et al., 1991; Jackson et al., 1991). We and others have noted that antibody sequences vary widely in terms of bacterial expression efficiency, and the expression level of 43C9 is relatively poor (Gibbs et al., 1991). Thus, the successful use of the bacteriophage T3 expression system in this case suggests that it may have general utility for other antibodies. In addition, the yield of purified single-chain antibody produced by our system (600–700 $\mu$g per liter of culture) compares favorably with that obtained from the *lac* promoter-based system constructed by Plückthun and co-workers (Plückthun, 1991; Skerra & Plückthun, 1991). The ability to express soluble single-chain antibodies might also allow genetic selection for catalytic activity at the level of bacterial colonies. This would significantly enhance our ability to screen large combinatorial libraries of antibody genes, complementing the existing assays for binding affinity (Posner et al., 1993).

There is substantial kinetic evidence for an acyl–antibody intermediate linked *via* a histidine residue. The pH–rate profile between pH 7 and 11 for *p*-nitrophenyl ester hydrolysis by wild-type 43C9 exhibited an apparent p$K_a$ of 9.0, which was assigned to a change in the rate-limiting step in the formation and breakdown of an intermediate (Benkovic et al., 1990). Titrations of ionizable groups involved in catalysis were not observed over this pH range. The two legs of the pH–rate profile were therefore assigned to rate-limiting deacylation of an acyl–antibody intermediate at pH values less than 9 and to rate-limiting *p*-nitrophenol release above pH 9. Since the p$K_a$ values for the ionization of unperturbed histidine, arginine, and tyrosine side chains are 6.5, 12.0, and 10.0, respectively (Stryer, 1981), the absence of observable ionizations in the binding site between pH 7 and 11 is not surprising. This is further evidence that the side chains of Tyr L32 and Tyr H95 do not play roles in catalysis by 43C9.

The properties of the H-L91-Q mutant are consistent with the assignment of His L91 as the active-site nucleophile in the wild-type protein. Substitution of nonnucleophilic glutamine at this position gave rise to a protein that had virtually the same binding affinity for ligands as the wild-type, but that possessed no detectable catalytic activity. Unfortunately, it was not possible to measure the $K_D$ value for substrate binding to this antibody due to the relatively rapid buffer-catalyzed decomposition of the ester substrates. In addition, experiments to determine the binding of amide **1a** are complicated by large inner filter effects and a high $K_D$ value (the $K_M$ value is 500 $\mu$M for the wild-type antibody). However, the virtually identical affinities for hapten, acid **2**, and *p*-nitrophenol **3b** argue that the mutation probably had little or no effect on substrate affinity and that the observed lack of turnover resulted from the loss of a side-chain nucleophile required for catalysis.

In contrast, our mutagenic studies revealed that substitution of His H35 with either Asn or Phe resulted in decreased ligand binding, as well as a loss of catalytic activity. Taken together, these results argue against a role for this residue in catalysis, but rather suggest a structural role. Furthermore, the consequences of replacing His H35 with other residues can be explained on the basis of previous structural studies of antibodies. The side chain of $V_H$ residue H35 is involved in an extensive hydrogen-bond network that includes a strongly conserved hydrogen bond to the indole nitrogen atom of framework residue Trp H47 (Roberts et al., 1994). The common occurrence of a polar residue at position H35 (Kabat et al., 1991) is also consistent with the importance of this hydrogen bond. In the 43C9 model, the His H35 N$\delta$ imidazole atom is aligned to form a hydrogen bond with Trp H47 (at a distance of 3.0 Å, Figure 5).

The mechanism for disruption of the antigen binding pocket when His H35 is replaced by Asn may involve a change in size of the side chain as well as a difference in positioning of polar side-chain atoms. His H35 underlies the side chains of Tyr H95 and Arg L96, which form the bottom of the antigen binding pocket (Figure 2). In the H-H35-N mutant, replacement by a smaller side chain should change the surface

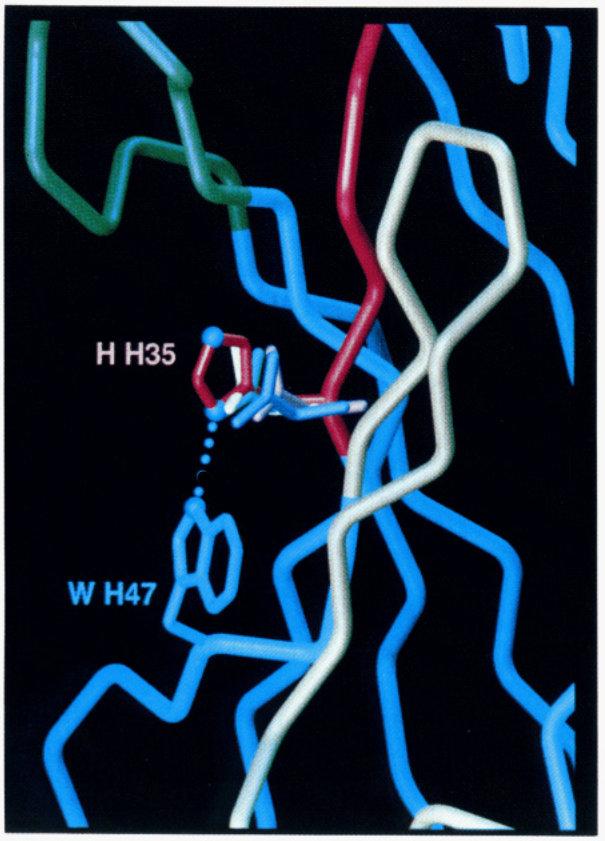


FIGURE 5: Side chain of residue His H35 aligned by a hydrogen bond with Trp H47. The backbone of the $V_H$ of 43C9 is superimposed onto the $V_H$ of known antibody structures by its conserved backbone structure. The Nδ of His H35 (red; blue spheres represent side-chain nitrogen atoms) forms a hydrogen bond to the Nε of Trp H47 (blue), aligning the His H35 side-chain ring in the same plane as the amide side chains of Asn H35 from the known antibody structures BV-04-01 (blue), 4-4-20 (magenta), D1.3 (light blue), and 36-71 (yellow).

upon which Arg L96 and Tyr H95 rest, thereby affecting the shape of the binding pocket. Furthermore, the resulting changes in the position and orientation of the Arg L96 guanidinium group could adversely affect its interactions with substrate and transition states, resulting in a loss of catalytic activity. The side-chain geometry of His H35 matches that of Asn H35 in crystallographically determined structures of other antibodies (Figure 5). Although the Oδ atom of the Asn residue adopts a geometry similar to that of the Nδ atom of His H35 in the 43C9 model, the other potential hydrogen-bonding atom of Asn, Nδ, cannot adopt the position of His H35 Nε. This change in the orientation of hydrogen-bonding atoms may also contribute to the decreased binding and loss of catalysis observed for the Asn H35 mutant.

Mutation of His H35 to Phe would eliminate the hydrogen bond between residues H35 and Trp H47. This change may subtly affect the shape of the antigen binding pocket in two ways. First, if the Trp H47 side chain retains its structurally conserved orientation in the mutant, the Phe H35 ring must rotate out of the plane of the His H35 imidazole ring to avoid steric interactions with the Trp H47 indole group. This movement may perturb the geometry of the adjacent Arg L96 side chain. Second, structural changes may occur at the bottom of the antigen binding site if the Trp H47 indole nitrogen forms a hydrogen bond to another group.

The above arguments suggest that while the side chain of His H35 does not directly participate in the catalytic mechanism of 43C9, it may not be possible to replace this amino acid with another residue and still maintain catalytic activity.

The lack of catalytic activity coupled with the nearly unchanged affinities for products displayed by R-L96-Q suggests that this residue is important for catalysis, as well as for hapten binding. The importance of Arg L96 in antigen binding by 43C9 has previously been demonstrated by the behavior of the R-L96-Q mutant (Roberts et al., 1994). In addition, the proximity of Arg L96 to the carbonyl oxygen of the substrate suggested that this residue might also play a role in catalysis by stabilizing the negatively charged tetrahedral transition states. In other words, Arg L96 might act as an oxyanion hole in the same way as in carboxypeptidase A and leucine aminopeptidase (Phillips & Fletterick, 1993). We believe that the positively charged side chain of Arg L96 plays two roles in catalysis: (1) to polarize the substrate carbonyl for nucleophilic attack and (2) to stabilize the anionic tetrahedral transition states by electrostatic interactions. Substitution of Arg L96 with glutamine, whose side chain is uncharged, precludes both of these effects.

The combination of the computer model of the 43C9 Fv fragment with the extensive kinetic investigations of the wild-type monoclonal antibody and the results of site-directed mutagenesis presented here afford a unique insight into antibody catalysis. The proposed mechanism of *p*-nitrophenyl ester hydrolysis by 43C9 is presented in Scheme 4, with the two key residues—His L91 and Arg L96—highlighted. Note that this representation was drawn for clarity and does not reproduce the three-dimensional positions of these side chains. Substrate binding orients the reactive carbonyl oxygen near the guanidinium group of Arg L96. Both hydrogen bonding and electrostatics are likely to be important in this interaction. This position also locates the carbonyl carbon near the side chain of His L91. The acyl intermediate is formed by attack of an imidazole nitrogen of His L91 on the substrate carbonyl. The side chain of Arg L96 provides an oxyanion hole for this tetrahedral transition state, and the liberated phenol remains bound to the antibody. This complex corresponds to the Ab·I detected kinetically (Benkovic et al., 1990). This intermediate breaks down by hydroxide attack to afford a stable ternary complex of antibody, acid, and phenol. These ligands are released sequentially to complete the catalytic cycle.

Substitutions for Tyr L32 and H95 were made in an effort to introduce general-acid catalysis into the mechanism and thereby increase the catalytic efficiency of 43C9. Unfortunately, the Y-L32-H mutant did not display enhanced catalytic activity against the *p*-chlorophenyl ester at pH 8.5; indeed, it proved *ca.* 2.5-fold less active than the wild-type. Since the $pK_a$ of the introduced His residue was expected to be approximately 7, the catalytic activity was also measured for this mutant as a function of pH. The pH–rate profile obtained between pH 8.5 and 6 had the same form as that of the wild-type, with no evidence for general-acid participation (D. B. Smithrud and S. J. Benkovic, unpublished results). The lack of participation of the introduced His residue is consistent with theoretical studies, which predict an extremely low barrier to phenoxide expulsion from a tetrahedral transition state for leaving groups with $pK_a$ values $<11$ [the $pK_a$ of *p*-chlorophenol is 9.38 (Gerstein & Jencks, 1964)] (Guthrie, 1991). Amide hydrolysis assays were not performed on this mutant owing to the low quantities of protein available.

The proximity of the side-chain hydroxyl of Tyr H95 to one of the antigen's phosphonamidate oxygens (Roberts et al., 1994) suggested that this residue might play a role in the catalytic mechanism. The results obtained from the Y-H95-F

mutant, however, do not support an essential role for this residue. Instead, the small decrease observed in the $k_{cat}$ value suggests that a major role of Tyr H95 may again be to assist in substrate orientation within the active site. It was originally hoped that replacing Tyr H95 with histidine would locate a general-acid catalyst in the vicinity of the tetrahedral intermediate while introducing only a modest change in side-chain volume. The lowered catalytic activity of the Y-H95-H mutant was therefore unexpected. The affinities of this mutant for the three ligands were nearly the same as those of the wild-type, suggesting that the active site remained largely intact. However, the possibility that these ligands were bound with the same affinities but in a different and nonproductive manner cannot be ruled out.

Antibody 43C9 has provided a unique opportunity for exploring antibody catalysis. The combination of the computer model for the 43C9 Fv structure and the results of previous kinetic investigations has enabled detailed predictions to be made concerning the contributions of individual amino acids to both binding and catalysis. The current method for producing the 43C9 single-chain antibody in *E. coli* has allowed us to test some of these predictions using the technique of site-directed mutagenesis. This technology will also allow for other structural and functional studies. The milligram quantities of single-chain antibody required for X-ray crystallography are now easily accessible. In addition, its production in a bacterial host will permit the incorporation of stable isotopes such as $^{13}C$ and $^{15}N$ for NMR studies. Finally, the availability of a structural model and an efficient means of protein expression open the possibility of engineering a derivative of 43C9 with novel characteristics.

## ACKNOWLEDGMENT

We thank Qing Zhang for assisting in preliminary experiments, Michael Pique and Alexandre Shah for help with computer graphics, and Irene Lee, Tom Mueller, Bruce Posner, Michele Rollence, and John Tainer for many helpful discussions. Figures 2 and 5 were rendered with the AVS graphics program (Advanced Visual Systems, Inc., Waltham, MA) on a Kubota Denali graphics workstation.

## REFERENCES

Barshop, B. A. R., Wrenn, F., & Freiden, C. (1983) *Anal. Biochem. 130*, 134–145.

Benkovic, S. J. (1992) *Annu. Rev. Biochem. 61*, 29–54.

Benkovic, S. J., Adams, J. A., Borders, C. L., Jr., Janda, K. D., & Lerner, R. A. (1990) *Science 250*, 1135–1139.

Gerstein, J., & Jencks, W. P. (1964) *J. Am. Chem. Soc. 86*, 4655–4663.

Gibbs, R. A., Posner, B. A., Filpula, D. R., Dodd, S. W., Finkelman, M. A. J., Lee, T. K., Wroble, M., Whitlow, M., & Benkovic, S. J. (1991) *Proc. Natl. Acad. Sci. U.S.A. 88*, 4001–4004.

Gibbs, R. A., Benkovic, P. A., Janda, K. D., Lerner, R. A., & Benkovic, S. J. (1992) *J. Am. Chem. Soc. 114*, 3528–3534.

Glockshuber, R., Stadlmüller, J., & Plückthun, A. (1991) *Biochemistry 30*, 3049–3054.

Guthrie, J. P. (1991) *J. Am. Chem. Soc. 113*, 3941–3949.

Ho, S. N., Hunt, H. D., Horton, R. M., Pullen, J. K., & Pease, L. R. (1989) *Gene 77*, 51–59.

Jackson, D. Y., Prudent, J. R., Baldwin, E. P., & Schultz, P. G. (1991) *Proc. Natl. Acad. Sci. U.S.A. 88*, 58–62.

Janda, K. D., Schloeder, D., Benkovic, S. J., & Lerner, R. A. (1988) *Science 241*, 1188–1191.

Janda, K. D., Ashley, J. A., Jones, T. M., McLeod, D. A., Schloeder, D. M., Weinhouse, M. I., Lerner, R. A., Gibbs, R. A., Benkovic, P. A., Hilhorst, R., & Benkovic, S. J. (1991) *J. Am. Chem. Soc. 113*, 291–297.

Kabat, E. A., Wu, T. T., Perry, H. M., Gottesman, K., & Foeller, C. (1991) *Sequences of Proteins of Immunological Interest*, 5th ed., National Institutes of Health, Bethesda, MD.

Lerner, R. A., Benkovic, S. J., & Schultz, P. G. (1991) *Science 252*, 659–667.

McManus, S., & Riechmann, L. (1991) *Biochemistry 30*, 5851–5857.

Phillips, M. A., & Fletterick, R. J. (1993) *Curr. Opin. Struct. Biol. 2*, 713–720.

Plückthun, A. (1991) *Bio/Technology 9*, 545–551.

Posner, B., Lee, I., Itoh, T., Pyati, J., Graff, R., Thorton, G. B., La Polla, R., & Benkovic, S. J. (1993) *Gene 128*, 111–117.

Riechmann, L., Cavanagh, J., & McManus, S. (1991) *FEBS Lett. 287*, 185–188.

Roberts, V. A., Stewart, J. D., Benkovic, S. J., & Getzoff, E. D. (1994) *J. Mol. Biol. 235*, 1098–1116.

Sambrook, J., Fritsch, E. F., & Maniatis, T. (1989) *Molecular Cloning. A Laboratory Manual*, Cold Spring Harbor Laboratory Press, Cold Spring Harbor, NY.

Skerra, A., & Plückthun, A. (1991) *Protein Eng.*, 971–979.

Stewart, J. D., & Benkovic, S. J. (1993) *Chem. Soc. Rev. 22*, 213–219.

Stewart, J. D., Liotta, L. J., & Benkovic, S. J. (1993) *Acc. Chem. Res. 26*, 396–404.

Stryer, L. (1981) *Biochemistry*, p 80, W. H. Freeman and Company, New York.

Taira, K., & Benkovic, S. J. (1988) *J. Med. Chem. 31*, 129–137.

Whitlow, M., & Filpula, D. (1991) *Methods (San Diego) 2*, 97–105.

Yanisch-Perron, C., Viera, J., & Messing, J. (1985) *Gene 33*, 103–119.